NANO LETTERS

2008
Vol. 8, No. 1
142−146

Exciton Dissociation and Stark Effect in the Carbon Nanotube Photocurrent Spectrum

Aditya D. Mohite, Prasanth Gopinath, Hemant M. Shah, and Bruce W. Alphenaar*

Department of Electrical and Computer Engineering, University of Louisville, Louisville, Kentucky 40292

Received September 4, 2007; Revised Manuscript Received November 2, 2007

ABSTRACT

The field-dependent photocurrent spectrum of individual carbon nanotubes is measured using a displacement photocurrent technique. A series of peaks is observed in the photocurrent corresponding to both excitonic and free carrier transitions. The photocurrent peak corresponding to the ground state exciton increases by a factor of 200 beyond a critical electric field, and shows both red and blue shifts depending on the field regime. This provides evidence for field-induced mixing between excitonic and free carrier states.

Quantum confinement and electron−electron interactions produce a unique set of optical phenomenon in semiconductor carbon nanotubes not observed in three-dimensional semiconductors.[1] Carbon nanotubes have a series of van Hove singularities in the electronic density of states that allow for optical excitation across a spectrum of transition energies.[2] The band-to-band transition energies are dependent on the nanotube diameter and chirality, and have been used for nanotube identification. For the most part, however, optical absorption in nanotubes is not expected to occur via band-to-band transitions, but through the creation of bound electron hole pairs, or excitons.[3−6] This surprising prediction has been confirmed experimentally through the observation of phonon sidebands,[7] two-photon luminescence spectroscopy,[8,9] and later through photocurrent spectroscopy.[10] The oscillator strength for exciton formation is typically many times higher than that for the formation of free electron hole pairs.[11] The excitonic optical transition energy differs from the band-to-band transition energy by the exciton binding energy, which can be as high as 500 meV.

Recently, some effort has gone toward understanding the influence of electric field on the nanotube optical response. In three-dimensional semiconductors, electric field is known to cause a Stark shift in the absorption maximum and a modulation in the absorption coefficient.[12] For nanotubes, Perebeinos et al. predicted a strong modulation of the absorption spectra with increasing electric field.[13] The exciton formation rate due to impact ionization is also exponentially dependent on the electric field, and increases dramatically for potentials above the optical phonon energy.[14,15] Importantly, the electric field also provides a mechanism by which the excitonic states can be disassociated into free carriers (similar to the field-induced ionization observed in atomic systems).[16] Field-induced exciton dissociation should have a measurable effect on the nanotube photocurrent. At zero electric field, bound charge carriers cannot contribute to the photocurrent unless they disassociate into a free carrier state. Electric field provides a dissociation mechanism that effectively "turns-on" the ground-state excitonic transition in the photocurrent spectrum. In this way, free and bound charge transitions in the optical spectrum can be distinguished, and the influence of electric field on either type of transition can be explored.

Here, we describe the results of an innovative photocurrent measurement technique[17−19] that allows measurement of the excitation spectrum of individual nanotubes while applying large electric fields. Figure 1 shows our measurement setup. Individual single-wall nanotubes (SWNTs) are grown by chemical vapor deposition on an oxidized p^{++} silicon substrate (oxide thickness is 100 nm). Atomic force microscope imaging (Figure 1b) shows that the nanotube density is 3−6 SWNTs per 25 × 25 μm^2 area with an average nanotube diameter of 1.3 nm. A 25 nm thick layer of indium tin oxide (ITO) is deposited by electron beam evaporation, creating a transparent Schottky contact to the nanotubes. As shown in Figure 1a, the final device structure is a capacitor with a heavily doped silicon back electrode, a silicon dioxide dielectric, and an ITO top electrode. Applying a dc bias across the capacitor creates an electric field $\vec{F}$ perpendicular to the nanotube axis. We emphasize that we do not apply any bias across the length of the nanotube (parallel to the nanotube axis) as is done in a standard photocurrent

* Corresponding author. Phone: 502-852-1554. Fax: 502-852-8128. E-mail: brucea@louisville.edu.

10.1021/nl0722525 CCC: $40.75 © 2008 American Chemical Society
Published on Web 11/30/2007

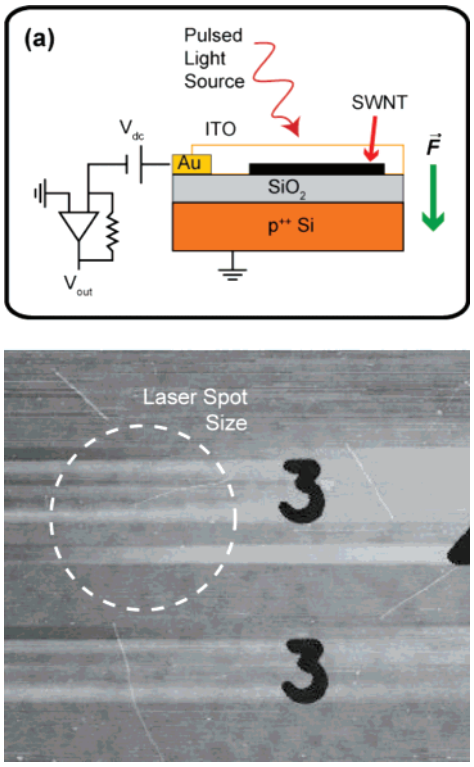

Figure 1. (a) Schematic drawing of the experimental setup. SWNTs are grown parallel to the sample surface. The displacement photocurrent is measured between the ground electrode and the ITO contacting the nanotubes. (b) Atomic force microscope image of the top surface of the device showing the nanotube density and laser spot size.

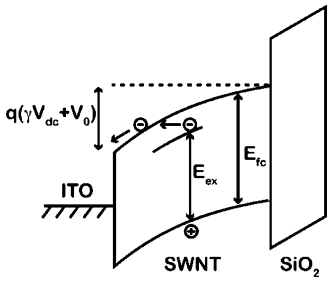

Figure 2. Simplified band diagram of the ITO/SWNT/oxide structure showing the lowest order free carrier E_{fc} and excitonic E_{ex} transitions.

experiment. To probe the nanotube photoexcitation spectrum, pulsed laser light is directed at a single carbon nanotube lying at the ITO/oxide interface. We use a Spectra-Physics optical parametric amplifier (OPA) pumped by a 130 fs pulsed Ti: sapphire laser with a repetition rate of 1 kHz. The excitation energy is tunable from 0.4 to 4 eV.

The mechanism for photoexcitation and charge carrier detection can be understood by considering the simplified band diagram shown in Figure 2. The lowest order free-carrier and excitonic transitions in the nanotube are denoted by E_{fc} and E_{ex}, respectively. V_o is the built-in potential that exists at the SWNT/ITO interface, which arises from the unequal chemical potential between the SWNT and ITO. If light is absorbed by a carbon nanotube to create electron hole pairs, the charge will tend to separate as a result of this built-in Schottky barrier potential. For a p-type nanotube, holes will drift into the ITO, while electrons will drift toward the oxide interface. The charge separation produces an ac displacement current across the ITO/Si capacitor, which can be measured with a lock-in amplifier, synched to the laser repetition rate. The displacement photocurrent signal requires optical excitation of charge carriers followed by physical separation of the excited charge. The technique is thus sensitive to optical excitations in which freely mobile charge carriers are created. Another advantage is that it is straightforward to characterize individual nanotubes by increasing the spacing between nanotubes on the sample surface so that it is larger than the laser spot size.

Application of electric field increases the band-bending across the carbon nanotube and thereby increases the carrier capture efficiency. Because of the capacitor structure, it is possible to apply large electric fields without generating appreciable dark current. We can make a rough estimate of the electric field across the nanotube for an applied bias V_{dc} by considering the nanotube as an insulator with a dielectric constant $\epsilon_{nt} = 3.3$[12] and thickness $T_{nt} = 1.3$ nm lying on the silicon dioxide insulator with dielectric constant $\epsilon_{ox} = 3.9$ and thickness $T_{ox} = 100$ nm. The electric field across the nanotube is then given by

$$F_{nt} = \frac{V_{dc}\epsilon_{ox}}{(T_{nt}\epsilon_{ox} + T_{ox}\epsilon_{nt})} \quad (1)$$

For a maximum applied bias of 32 V, this gives $F_{nt} = 3.7 \times 10^8$ V/m and a voltage drop across the width of the nanotube of $\gamma V_{dc} = 0.48$ V, where $\gamma = 0.015$ is the fraction of the applied bias that drops across the nanotube. While this is only a rough estimate, it shows that band-bending large enough to influence charge transport across the nanotube/ITO interface can easily exist. There are a number of uncertainties in this equation, including ϵ_{nt}, which can range from 2.6 to 3.3, and the exact nanotube diameter, which could be off by 0.1 nm or more.

Figure 3a shows the photocurrent measured for a typical nanotube at the ITO/oxide interface with an applied bias of $V_{dc} = 20$ V. A number of peaks are observed as a function of laser excitation energy. The diameter of the laser spot is approximately 5 μm, so that, on average, the laser illuminates less than one nanotube. Consequently, the photocurrent is negligible for the vast majority of the sample area: to obtain the spectrum shown here, the laser spot is first painstakingly scanned along the sample surface until a nanotube is found. Evidence that we are measuring an individual nanotube is provided by the polarization dependence of the photocurrent, shown in Figure 3b. Each of the four main peaks observed in the photocurrent show strong polarization dependence, and are maximized at the same polarization angle.

Comparison to absorbance spectroscopy measurements made on similarly prepared nanotube films[17,18] shows that the two highest magnitude peaks in Figure 3a correspond to the lowest energy E_{11}, and next higher energy E_{22} excitonic transitions in the absorbance spectrum. The photocurrent measured near the E_{22} transition is shown in detail in Figure

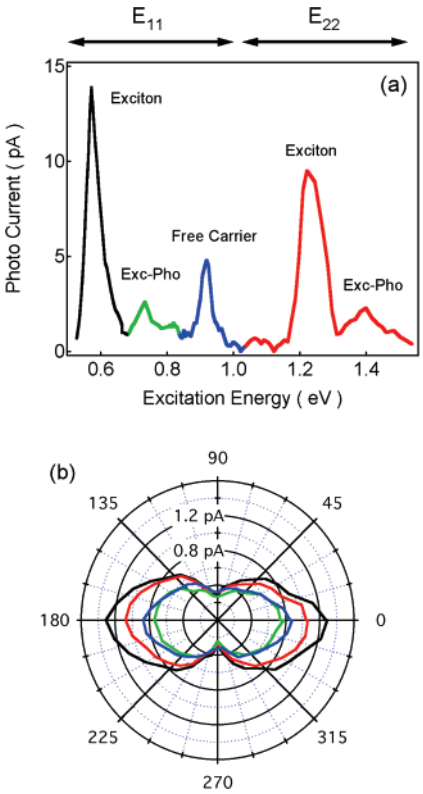

Figure 3. (a) Photocurrent versus excitation energy for an individual nanotube measured with 20 V dc bias across the capacitor. (b) Polarization angle dependence for the four largest photocurrent peaks.

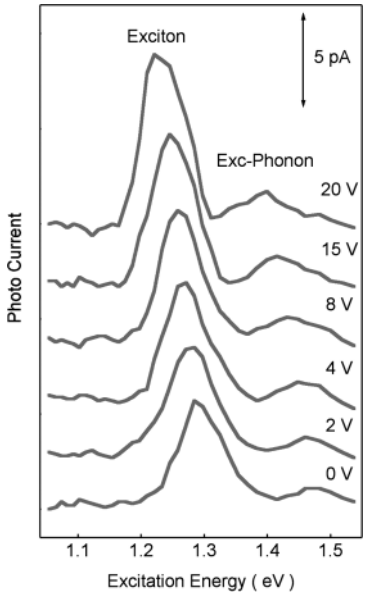

Figure 4. Photocurrent spectra versus excitation energy measured near the E_{22} excitonic transition for bias ranging from 0 to 20 V. Curves are offset for clarity.

4, for a series of dc biases ranging from 0 to 20 V (corresponding to electric fields across the nanotube ranging from 0 to 2.32 MV/m). A dominant peak is observed at around 1.28 eV, together with a satellite peak 185 meV above the main resonance. As has been described in the literature,[7] a satellite peak can arise from exciton−phonon coupling of

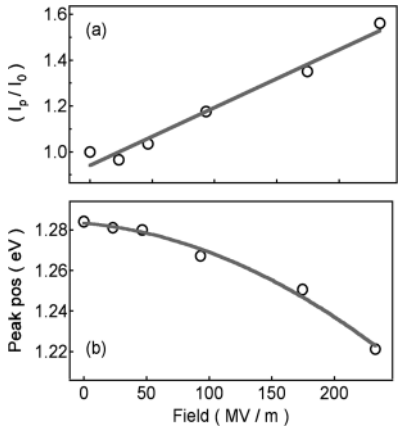

Figure 5. (a) Normalized photocurrent versus electric field for the E_{22} excitonic peak. (b) E_{22} excitonic peak position verses electric field; a quadratic fit to the data is shown.

the optically active exciton with the dipole-forbidden dark exciton. The LO phonon mode associated with C−C bond stretching mixes much more strongly with the light and dark excitonic states than with the free carrier state. This provides further evidence that the main peak corresponds to an excitonic state. Both peaks show a red shift with increasing electric field. Figure 5b shows the main E_{22} peak position as a function of electric field, and, as indicated by the solid line, a quadratic field dependence fits the data reasonably well. A quadratic field dependence is also observed in the quantum confined Stark effect for semiconductor quantum wells[20,21] (field perpendicular to the well) and, for nanotubes, has been predicted for electric field parallel to the nanotube axis.[13] The red shift is expected as long as mixing with the lowest energy band-to-band transition is not too strong, in which case a blue shift is possible.

Figure 5a shows the magnitude of the photocurrent (normalized with respect to the zero field value) for the main resonance as a function of electric field. The photocurrent increases approximately linearly with electric field, suggesting there is no appreciable barrier for the transmission of the charge into the ITO contact following photoexcitation of the carriers. It is expected that the E_{22} exciton decays rapidly into the lower energy continuum states where the charge can move freely through the sample.[7] Assuming ohmic conduction, the slope of the field dependence in Figure 5a is $\sigma A/I_0$, where σ is the transport conductivity, A is the cross-sectional area of the photoexcited region of the nanotube, and $I_0 = 5.7$ pA is the peak height at zero applied field. (The built in potential at the nanotube/ITO interface V_0 allows optically excited carriers to travel into the contact, even at zero bias.) A is given by the length of the nanotube illuminated by the laser (approximated by the laser spot diameter) multiplied by the nanotube diameter, or $(5 \times 10^{-6}$ m$)(1.3 \times 10^{-9}$ m$) = 6.5 \times 10^{-15}$ m^2. This gives a conductivity of $\sigma = 8.25 \times 10^{-4}\ \Omega^{-1}$ m^{-1}.

A very different field dependence is observed in the E_{11} excitonic regime. Figure 6a shows the photocurrent measured in the regime of the E_{11} exciton for a range of applied biases. At low bias, only a single peak is observed near 0.88 eV. At higher bias, a second peak emerges near 0.61 eV. The

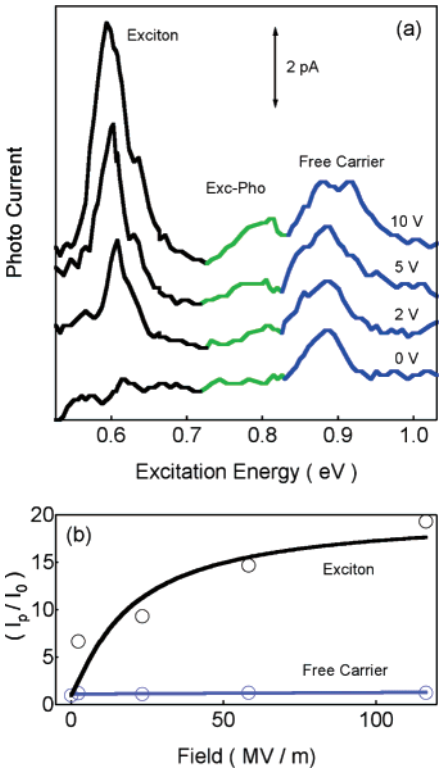

Figure 6. (a) Photocurrent versus excitation energy measured near the E_{11} exciton transition for bias ranging from 0 to 10 V. The curves are offset for clarity. The apparent splitting in the free carrier peak at 10 V is not reproduced in other devices. (b) Normalized photocurrent versus electric field of the excitonic and free carrier peaks.

magnitude of the lower energy peak increases with increasing bias and eventually overshadows the higher energy peak. Figure 6b shows the normalized photocurrent measured for both the lower and higher energy peaks. The higher energy peak changes little with applied field, while the lower energy peak shows a large increase. In addition, the lower energy peak is accompanied by a phonon satellite peak, which is approximately 185 meV higher in energy than the main peak position. (This is similar to the exciton−phonon satellite peak observed in the E_{22} spectrum). This suggests that the lower energy peak is the E_{11} excitonic state, while the higher energy peak is the ground-state free carrier transition. (This assignment also agrees with absorption measurements made on carbon nanotube films.[10]) A similar peak structure was observed in four different semiconducting nanotubes. We can extract the E_{11} exciton binding energy by taking the energy difference between the excitonic and band-to-band photocurrent peaks. For the spectra in Figure 6, this gives 0.274 eV, while binding energies ranged from 0.270 to 0.300 eV for the four nanotubes measured. These values agree with theoretical predictions, assuming a nanotube diameter of 1.3 nm and a dielectric constant $\epsilon_{nt} = 3.3$.[11,13,22]

The field dependence of the E_{11} excitonic transition can be understood using a recently described field-enhanced tunneling model,[10,23] which assumes a constant field across the width of the nanotube. As shown in Figure 2, the applied bias V_{dc} brings the energies of the free carrier and bound carrier states into alignment. Bound carriers can then

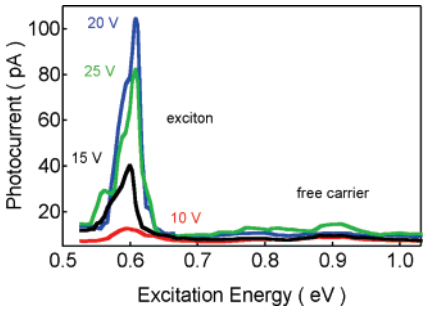

Figure 7. Photocurrent versus excitation energy measured near the E_{11} exciton transition for bias ranging from 10 to 25 V.

dissociate into free carriers by tunneling into the continuum through the barrier created by the exciton binding energy. Increasing the bias acts to reduce the tunnel barrier width and consequently increase the tunneling rate. In this case, the normalized photocurrent is given by

$$I_p/I_0 = \exp\left[\frac{4}{3}\frac{\sqrt{2m^*}}{q\hbar}\frac{E_b^{3/2}T_{nt}}{V_0}\frac{\gamma V_{dc}}{(V_0+\gamma V_{dc})}\right] \equiv \exp\left[\frac{a}{(1+b/V_{dc})}\right] \quad (2)$$

where $a = 4/3\ \sqrt{2m^*}/q\hbar\ E_b^{3/2}t\gamma/V_0$ and $b = V_0/\gamma$. Equation 2 can be simplified further by plugging in for the exciton binding energy $E_b = 0.3$ eV (given by the energy separation between the excitonic and free carrier peaks in Figure 6a), the nanotube thickness T_{nt} =1.3 nm, and the effective mass m^* (taken to be the free electron mass m_0). This gives $a = 1.46\ (\gamma/V_0) = 1.46/b$, leaving eq 2 with only one fitting parameter, b. The solid line in Figure 6b is a fit of eq 2 to the experimental data for $b = 0.48$. It is seen that the tunneling model provides a good description of the E_{11} exciton field dependence in the bias range 0−10 V (when plotting the data, bias has been converted to electric field, using eq 1). Using $b = 0.48$ from eq 2 and $\gamma = 0.015$ from eq 1 gives $V_0 = 7.3$ mV, which is not unreasonable for the built-in potential at the ITO/nanotube interface.

For higher electric fields, the tunneling model predicts that the photocurrent should saturate; however, this behavior is not observed. Figure 7 shows the photocurrent spectra near the E_{11} excitonic transition for biases ranging from 10 to 25 V. In Figure 8a, the magnitude of the excitonic peak is plotted as a function of electric field. At field strengths of 150 MV/m, the exciton peak increases by almost an order of magnitude. No similar increase is observed in the free carrier peak, which becomes dwarfed by the excitonic peak. The signal reaches a maximum at a field of 200 MV/m, and then decreases somewhat at higher fields.

A clue to understanding this behavior is provided by the field dependence of the E_{11} peak position, (shown in Figure 8b). For the low field range of 0−120 MV/m, the peak position shifts to lower energy and is well described by a quadratic field dependence. The E_{11} and E_{22} peaks show a similar field dependence in this regime; however, the E_{11} Stark shift is substantially larger than the E_{22} Stark shift (in

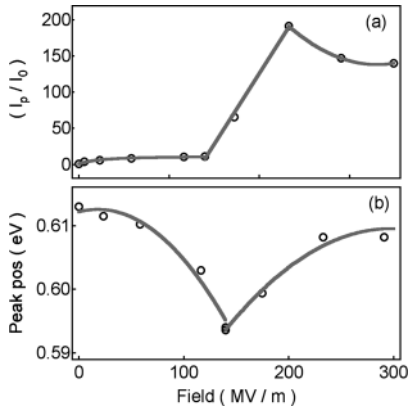

Figure 8. (a) Normalized photocurrent and (b) excitonic peak position versus electric field for the E_{11} excitonic peak in the high field regime. Quadratic fits to the peak position are shown.

agreement with predictions for electric field parallel to the nanotube axis).[13] At 120 MV/m, just when the peak magnitude is observed to increase sharply, the Stark shift changes direction from red to blue. A second semiconducting nanotube measured in the high field regime showed similar behavior. The data suggest that, at some critical electric field, increased mixing occurs between the excitonic and free carrier states. This would lead to a large increase in the photocurrent, as well as a changeover to a blue shift, as the Stark shift of the continuum states becomes increasingly dominant. Perebeinos et al. predicted mixing between the excitonic and free carrier states occurring for electric field parallel to the nanotube; however, the perpendicular field case that we measure here has yet to be analyzed theoretically. We also note that our data looks similar to results observed in field-enhanced ionization of atomic systems in which level crossings lead to a rapid increase and then decrease of the ionization rate.

In conclusion, the influence of perpendicular electric field on the excitonic and free carrier transitions in carbon nanotubes is explored using a photocurrent technique. As observed in nanotube films, electric field causes the dissociation of excitons through field-assisted tunneling into the free carrier states. An order of magnitude increase in the excitonic peak is observed beyond a critical electric field, at which point the Stark shift also changes sign. This provides evidence for field-induced mixing of excitonic and free carrier states in carbon nanotubes.

Acknowledgment. The authors thank R.W. Cohn and J. Kielkopf for valuable discussions. Funding provided by ONR (No. N00014-06-1-0228) and NASA (No. NCC 5-571).

References

(1) Dresselhaus, M., Dresselhaus, G., Avouris, P., Eds. *Carbon Nanotubes: Synthesis, Structure, Properties and Applications*; Springer: Berlin, 2001.
(2) Kataura, H.; Kumazawa, Y.; Maniwa, Y.; Umezu, I.; Suzuki, S.; Ohtsuka, Y.; Achiba, Y. *Synth. Met.* **1999**, *103*, 2555.
(3) Ando, T. *J. Phys. Soc. Jpn.* **1997**, *66*, 1066.
(4) Avouris, Ph. *MRS Bull.* **2004**, *29*, 403.
(5) Spataru, C. D.; Ismail-Beigi, S.; Benedict, L. X.; Louie, S. G. *Phys. Rev. Lett.* **2004**, *92*, 077402.
(6) Korovyanko, O. J.; Sheng, C.-X.; Vardeny, Z. V.; Dalton, A. B.; Baughman, R. H. *Phys. Rev. Lett.* **2004**, *92*, 17403.
(7) Freitag, M.; Martin, Y.; Misewich, J. A.; Martel, R.; Avouris, Ph. *Nano Lett.* **2003**, *3*, 1067.
(8) Wang, F.; Dukovic, G.; Brus, L. E.; Heinz, T. F. *Science* **2005**, *308*, 838.
(9) Maultzsch, J.; Pomraenke, R.; Reich, S.; Chang, E.; Prezzi, D.; Ruini, A.; Molinari, E.; Strano, M.; Thomsen, C.; Lienau, C. *Appl. Phys. Lett.* **2005**, *72*, 241402.
(10) Mohite, A.; Lin, J.-T.; Sumanasekera, G.; Alphenaar, B. W. *Nano Lett.* **2006**, *6* (7), 1369.
(11) Perebeinos, V.; Tersoff, J.; Avouris, P. *Phys. Rev. Lett.* **2004**, *92*, 257402.
(12) Keldysh, L. V. *Zh. Eksp. Teor. Fiz.* **1958**, *34*, 1138; *Sov. Phys. JETP* **1958**, *7*, 788.
(13) Perebeinos, V.; Avouris, P. *Nano Lett.* **2007**, *7*, 609.
(14) Perebeinos, V.; Avouris, P. *Appl. Phys. Lett.* **2006**, *74*, 121410.
(15) Bosnick, K.; Gabor, N.; McEuen, P. *Appl. Phys. Lett.* **2006**, *89*, 163121.
(16) Miller, L.; Kash, M.; Kleppner, D. *Phys. Rev. Lett.* **1978**, *41* (2), 103.
(17) Mohite, A.; Sumanasekera, G. U.; Hirahara, K.; Bandow, S.; Iijima, S.; Alphenaar, B. W. *Chem. Phys. Lett.* **2005**, *412*, 190.
(18) Mohite, A.; Gopinath, P.; Chakraborty, S.; Alphenaar, B. W. *Appl. Phys. Lett.* **2005**, *86*, 061114.
(19) Vaddiraju, S.; Mohite, A.; Chin, A.; Meyyappan, M.; Sumanasekera, G. U.; Alphenaar, B. W.; Sunkara, M. K. *Nano Lett.* **2005**, *5*, 1625.
(20) Miller, D. A. B.; Chemla, D. S.; Damen, T. C.; Gossard, A. C.; Wiegmann, W.; Wood, T. H.; Burrus, C. A. *Phys. Rev. Lett.* **1984**, *53*, 2173.
(21) Miller, D. A. B.;Chemla, D. S.; Schmitt-Rink, S. *Phys. Rev. B* **1983**, *33*, 6976.
(22) Dukovic, G.; Wang, F.; Song, D.; Sfeir, M. Y.; Heinz, T. F.; Brus, L. E. *Nano Lett.* **2005**, *5* (11), 2314.
(23) Moses, D.; Wang, J.; Heeger, A. J.; Kirova, N.; Brazovski, S. *Proc. Natl. Acad. Sci. U.S.A.* **2001**, *98*, 13496.

NL0722525